JACS
JOURNAL OF THE AMERICAN CHEMICAL SOCIETY
Article
pubs.acs.org/JACS

Biofunctionalization of Si(111)7×7 by "Renewable" L-Cysteine Transitional Layer

Fatemeh R. Rahsepar, Lei Zhang, Hanieh Farkhondeh, and K. T. Leung*

WATLab and Department of Chemistry, University of Waterloo, Waterloo, Ontario N2L 3G1, Canada

Supporting Information

ABSTRACT: Surface functionalization of an inorganic surface with bio-organic molecules is often aimed at creating a "permanent" bio-organic surface with receptor functional groups. We show here that L-cysteine can be used to transform a highly reactive Si(111)7×7 surface to not just a permanent bio-organic surface but also a semipermanent (or renewable) and a temporary bio-organic surfaces by manipulating the exposure. In the early growth stage, the strong bonding between the first cysteine adlayer and the Si substrate through Si−N or Si−S linkages in unidentate or bidentate arrangement provides permanent biofunctionalization by this interfacial layer. This interfacial layer can be used to build a transitional layer (second adlayer) mediated by interlayer vertical hydrogen bonding between an amino group and a carboxylic acid group. Further exposure of cysteine eventually leads to a zwitterionic multilayer film involving electrostatic interactions between cation ($-NH_3^+$) and anion moieties ($-COO^-$). The interlayer hydrogen bonding therefore provides temporary trapping of bio-organic molecules as the second transitional layer that is stable up to 175 °C. This transitional layer can be easily removed by annealing above this temperature and then regenerated with the same molecular layer or a different one by "renewing" the interlayer hydrogen bonds. We also illustrate coverage-dependent adsorption structures of cysteine, from bidentate to unidentate attachments and to self-assembled multimers, involving formation of intralayer horizontal N···H−O hydrogen bonds, by combining our X-ray photoemission data with the local density-of-state images obtained by scanning tunnelling microscopy.

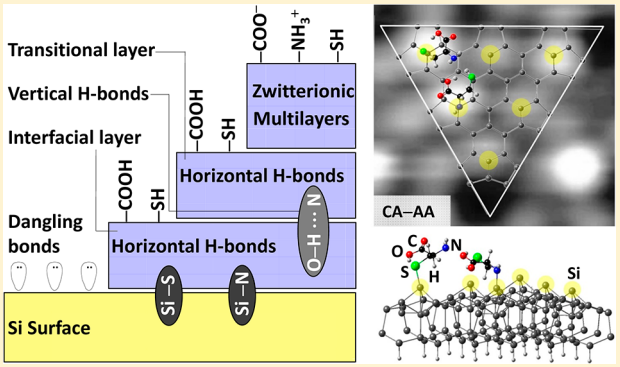

INTRODUCTION

Site-specific chemistry of bio-organic molecules on semiconductor surfaces has attracted much recent attention in nanotechnology because it enables nanoscale conversion of an inorganic surface to an organic surface with opportunities for introducing multiple types of bonding. Incorporating functions by direct organic molecular attachment to semiconductor materials through both organic reactions in dry (vacuum) or wet conditions (solution) can lead to new emerging technological applications, as in the development of hybrid organic−semiconductor devices, three-dimensional memory chips, silicon-based nanoscale or biological sensors, and nanolithography.[1−8] An important goal in organosilicon surface chemistry is to modify the electronic properties of the silicon surfaces and devices with organic molecules. Chemical attachment of organic molecules to a reconstructed silicon surface, that is, organic functionalization, by taking advantage of the different reactivities of surface sites provides the necessary control. The Si(111)7×7 surface offers an ideal two-dimensional template with directional dangling bonds not only for anchoring and supporting metallic adsorbates such as nanoclusters[9] but also for interacting with simple "benchmark" bio-organic molecules, including amino acids (e.g., glycine),[10] peptides (e.g., glycylglycine),[11] and DNA-base molecules (e.g., adenine and thymine).[12,13] Our early studies have shown that bio-organic molecules including more than one functional group can be used to exploit site-specific chemistry of the Si(111)7×7 surface through competitive reactions among different functional groups with the Si surface dangling bonds.[12−15] Because these bio-organic molecules invariably contain moieties that can be linked to one another by intra- and interlayer hydrogen bonding, a new opportunity of creating not just permanent but indeed semipermanent (or renewable) biofunctionalization can be realized by manipulating these hydrogen bonds.

Fundamental understanding of the interactions of organic molecules with Si surface sites is the key to controlling the functionalization of semiconductor surfaces. These interactions at the interface can be typically categorized into longer-range noncovalent interactions and shorter-range covalent bonding. Through use of the weaker noncovalent interactions, including electrostatic interaction between statically charged species or molecular sites, hydrogen bonding, van der Waals forces, $\pi-\pi$ interactions, and hydrophilic binding, many new self-assembled structures have been produced. In contrast to the longer-range

Received: September 8, 2014
Published: November 6, 2014

   dx.doi.org/10.1021/ja509264t | J. Am. Chem. Soc. 2014, 136, 16909−16918

interactions in these weakly interacting systems, strong shorter-range chemical bonds provide the essential binding in many interfacial structures on semiconductor surfaces and in devices functionalized with bio-organic molecules.[1,3,7,8]

Amino acids are ideal model molecules for investigating these long-range and short-range interactions with the Si surface, because they are the building blocks of proteins and as such represent one of the most important classes of biologically active molecules. They are also multifunctional molecules containing several different types of functional groups, and they therefore provide ideal systems for comparative studies of the relative strengths of interactions arising from different functional groups. Of the 20 naturally occurring amino acids, only cysteine ($C_\gamma OOHC_\alpha HNH_2C_\beta H_2SH$) contains a thiol (−SH) group, in addition to the carboxylic acid (−COOH) and amino ($-NH_2$) functional groups. Cysteine is a strong ligand for transition metals, making it a potential candidate of active materials for trace metal sensing. The adsorption of cysteine on (single-crystal) surfaces of a variety of metals, including copper,[16] silver,[17] and gold,[18] has been investigated. Cysteine was found to normally bind to the metal in the form of a thiolate.[16−18] Depending on the nature of the surface, the other two functional groups also play an important role in attaching cysteine to the surface. For example, in a recent study of cysteine adsorption on a semiconductor surface, the deprotonated carboxylic group was reported to be bound to the 5-fold coordinated Ti surface sites on rutile TiO_2(110).[19] Furthermore, carboxylic acid and amino groups enable cysteine film growth through the formation of the intra- and interlayer hydrogen bonding.

To date, there is only one report on cysteine adsorption on the Si(111)7×7 surface. In particular, Huang et al. studied cysteine adsorption on Si(111)7×7 by high-resolution electron energy loss spectroscopy and X-ray photoelectron spectroscopy (XPS), and they concluded the coexistence of two chemisorption states, including a unidentate adspecies through the cleavage of an O−H bond and a bidentate adspecies with new Si−N and Si−O linkages (with two Si adatoms).[20] However, the cysteine molecule, with an NH_2 to OH separation of 3.66 Å, proves to be physically too small to realize the proposed bidentate structure, through the amino and hydroxyl groups, that bridge two adjacent Si adatoms across the dimer wall or in the same half unit cell, with a separation of 6.77 and 7.66 Å, respectively. Here, we present the first STM investigation of the adsorption configurations of cysteine on Si(111)7×7 as a function of coverage at room temperature under ultrahigh vacuum conditions. By correlating these density of states images with the chemical state information provided by XPS, we determine the relative reactivity and selectivity of different surface sites toward the three functional groups in cysteine. We observe three different growth stages of cysteine, from chemisorbed adstructures in the interfacial layer (first adlayer) to transitional layer (second adlayer) to zwitterionic multilayers in the nanofilm. We further study the room-temperature durability and thermal evolution, particularly the stability of the transitional layer and zwitterionic multilayer film, on the reconstructed Si(111) using XPS. Of particular interest is that the interlayer hydrogen bonding allows the transitional layer to be used as a renewable layer that can be removed and regenerated by manipulating the annealing−exposure cycle. By correlating, for the first time, the chemical-state information provided by XPS with the high-resolution filled-state STM images at very low exposure of cysteine, we show that the bidentate attachment of cysteine is through Si−S and Si−N linkages with the (center-adatom, center-adatom) pair across the dimer walls of the 7×7 surface (in contrast to what was proposed earlier by Huang et al.).[20] Furthermore, the empty-state STM images reveal the formation of intralayer horizontal hydrogen-bonds (side-by-side) and interlayer vertical hydrogen-bonds (head-to-tail), respectively, within and between adsorbed unidentate cysteine molecules in the interfacial and transitional layers. These site-specific surface interactions and intra- and interlayer hydrogen bonding provide the important mechanism for different cysteine growth stages on the 7×7 surface. The biofunctionalization selectivity of the silicon surface arising from these growth stages is easily controlled by cysteine exposure, which offers new opportunities for sensing and molecular trapping applications of other bio-organic molecules and trace transition metals.

EXPERIMENTAL DETAILS

The experiments were carried out in a custom-built multichamber ultrahigh vacuum system (Omicron Nanotechnology, Inc.), with a base pressure greater than 5×10^{-11} mbar. The analysis chamber was equipped with a SPHERA hemispherical electron analyzer, monochromatized Al Kα source (1486.7 eV photon energy), and 7-channeltron detector assembly for XPS, along with a variable-temperature scanning probe microscope for atomic-resolution STM imaging. The organic molecular beam epitaxy (MBE) chamber was fitted with a low-temperature organic effusion cell (Dr. Ebert MBE-Komponenten GmbH) for cysteine deposition. Single-side polished n-type Si(111) chips (11×2 mm^2, 0.3 mm thick) with a resistivity of 5 mΩ cm (Virginia Semiconductors, Inc.) were employed as the substrates. A sharp contaminant-free Si(111)7×7 reconstructed surface was prepared by direct-current resistive heating at 400 °C overnight followed by flash-annealing at ∼1200 °C for 10 s, and the quality of the surface was validated by STM and XPS. All STM images were obtained at room temperature using a sharp electrochemically etched W tip and a constant tunneling current of 0.2 nA with appropriate sample bias voltages (negative bias for filled-state imaging and positive bias for empty-state imaging).

Cysteine (99.5% purity, Fluka), with a normal melting point at 240 °C, was exposed to the 7×7 substrate with the effusion cell held at 140 °C[21] and the deposition chamber pressure at 2×10^{-9} mbar. The cysteine powders in the effusion cell have been outgassed thoroughly overnight, prior to the deposition. The amount of deposited cysteine was controlled by the exposure time. The molecular identity and integrity of cysteine during exposure were confirmed by their cracking patterns, collected in situ with a quadrupole mass spectrometer (Stanford Research System RGA-300), and found to be in good accord with the literature.[22] Although the absolute coverage of cysteine could in principle be obtained directly from STM images for low exposure (for which the 7×7 pattern remains visible), deposition time was used here to indicate the relative exposure of cysteine due to the wide range of exposures employed in the present study.

For the film growth experiments, cysteine was deposited cumulatively on the same Si(111)7×7 substrate and STM images were collected after each exposure. The corresponding Si 2p, N 1s, C 1s, O 1s, S 2p, and S 2s XPS spectra were recorded with a pass energy of 20 eV, which gave an effective line width of 0.7 eV full width at half-maximum (fwhm) for the Ag $3d_{5/2}$ photoline at 368.3 eV. The spectra were fitted with Gaussian−Lorentzian line shapes (70% Gaussian and 30% Lorentzian) along with the Shirley background using the Casa-XPS software, and the binding energies are referenced to the Si $2p_{3/2}$ peak of bulk Si at 99.3 eV. For the thermal evolution experiments, as-grown thick cysteine films were annealed sequentially by resistive heating of the sample holder from 85 to 285 °C for 600 s, with the temperature monitored by a thermocouple located a few millimeters from the sample. We have also measured the core-level spectra of cysteine powders, in which case an electron neutralizer was employed to compensate the minor charging during the measurement. The

dx.doi.org/10.1021/ja509264t | J. Am. Chem. Soc. 2014, 136, 16909−16918

Scheme 1. Ball-and-Stick Models of (a) Neutral and (b) Zwitterionic Structures of Cysteine, and (c−g) Dimer Structures Resulting from Formation of Various H-Bonds (marked by the dashed lines) between Different Types of Functional Groups of Two Cysteine Molecules in the Gas Phase[a]

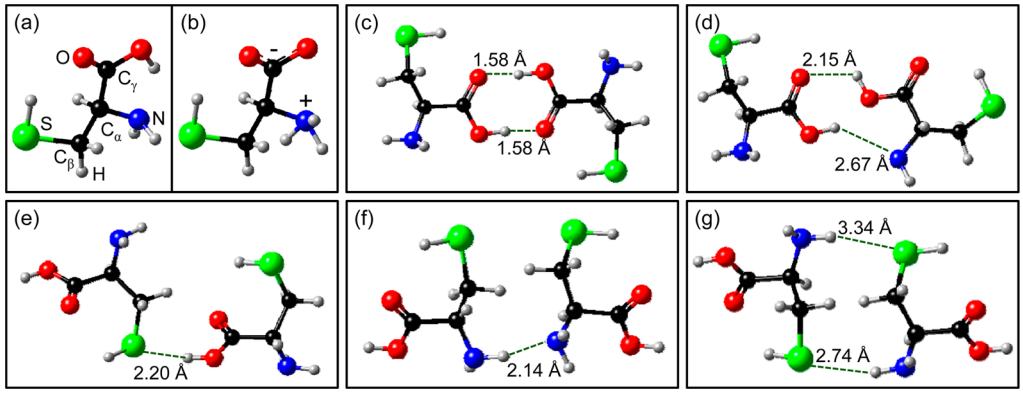

[a]These models are generated by DFT calculations.

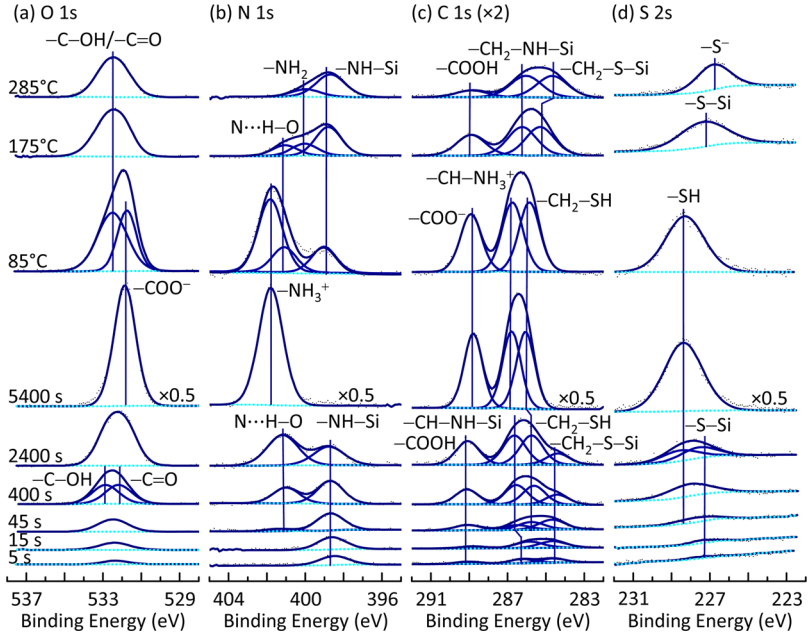

Figure 1. Evolution of (a) O 1s, (b) N 1s, (c) C 1s, and (d) S 2s XPS spectra of cysteine deposited on Si(111)7×7 as a function of exposure time (5−5400 s) and of the as-deposited 5400 s cysteine film upon annealing to 85, 175, and 285 °C.

binding energy scale of the powder spectra was calibrated with respect to that of the corresponding multilayer films by aligning the main N 1s feature (Supporting Information, Figure S1). After appropriate peak fitting of the observed spectral features, the ratios of peak areas could be used to determine the relative compositions of the chemical states.

RESULTS AND DISCUSSION

While cysteine exists as the neutral form in the gas phase (Scheme 1a),[23] the zwitterionic structure (Scheme 1b), with the protonated amino group ($-NH_3^+$) and deprotonated carboxylic group ($-COO^-$), is the most stable form in both aqueous solution and the solid state.[24] To analyze the chemical state evolution of cysteine nanofilm growth from submonolayer to multilayers on Si(111)7×7 and to investigate their stability at both room and evaluated temperatures in ultrahigh vacuum conditions, we conducted XPS experiments. Figure 1 shows the O 1s, N 1s, C 1s, and S 2s spectra of cysteine films as a function of exposure time, with their corresponding peak positions and assignments of the fitted features given in Tables S1 and S2 (Supporting Information). It should be noted that because the S 2p spectrum partially overlaps with one of the plasmon peaks of Si located at ∼168.0 eV (Supporting Information, Figure S2),[25] we have chosen S 2s for the present work. At very low exposures of 5−15 s, the N 1s spectra (Figure 1b) show only one peak at 398.7 ± 0.1 eV, attributed to a N−Si bond, which indicates that cysteine undergoes N−H dissociative adsorption on Si(111)7×7. This is in good accord with the N 1s feature at 398.8−399.1 eV found for chemisorption of dimethylamine,[26] pyrazine,[27] hexylamine,[28] 1,4-phenylenediamine, aniline,[29] glycine,[10] and glycylglycine[11] via N−H bond cleavage on Si surfaces. There is no sign of any neutral amino group ($-NH_2$) with a binding energy at ∼400.0 eV.[19] Our S 2s feature found at 227.4 eV in the present work is consistent with the Si−S linkage of chemisorbed cysteine, which indicates direct interaction of the S atom with the Si surface dangling bond. Because Si is less electronegative than H,[30] the S atom at the Si−S interface is anticipated to be more negatively charged than

dx.doi.org/10.1021/ja509264t | J. Am. Chem. Soc. 2014, 136, 16909−16918

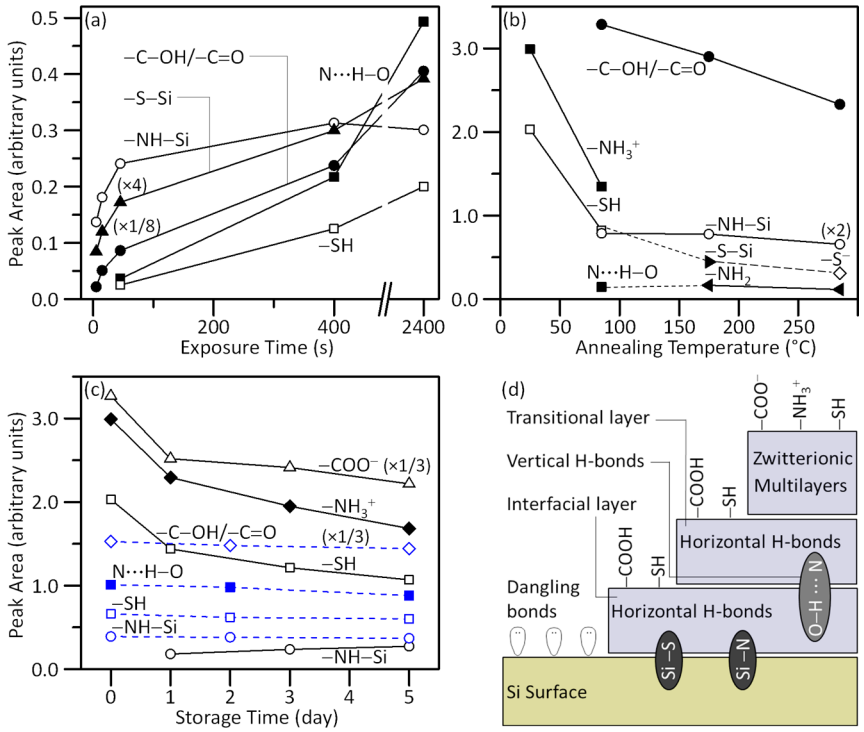

Figure 2. Peak areas of various O 1s, N 1s, C 1s, and S 2s features (a) for different cysteine exposure times and for a multilayer cysteine film (obtained with 5400 s exposure, solid lines) and a transitional layer (obtained by annealing the multilayer film at 85 °C for 20 min, dashed lines) as functions of (b) annealing temperature and (c) storage time in ultrahigh vacuum condition. (d) Schematic bonding model of available surface functional groups and intra- and interlayer interactions for the interfacial layer, transitional layer, and the multilayer film of cysteine on Si(111)7×7.

that in the thiol group and consequently to have a smaller binding energy than the S atom in an intact thiol group, with S 2s at 228.4 eV. This is in marked contrast to the work by Huang et al.,[20] who reported an intact thiol group for both physisorption and chemisorption of cysteine on Si(111)7×7. Furthermore, our assignment is also in good accord with Si–S species, with the S 2s feature at 227.3 eV, found for benzenethiol and diphenyl disulfide on the Si(001).[31] The results of N 1s and S 2s spectra therefore clearly show that for the lowest exposure (i.e., the interfacial layer), cysteine anchors on the Si surface through dissociation of both amino and thiol groups in a bidentate arrangement, because neither the XPS feature corresponding to intact N–H nor that corresponding to a S–H bond is observed. This bonding arrangement of the interfacial layer is also in good agreement with the information deduced from both filled-state and empty-state STM images (to be discussed below). Figure 1c shows three fitted C 1s peaks at 284.7, 286.3, and 289.2 eV, which can be attributed to the alkyl carbon atoms in C–S and C–N moieties and to the carbonyl C in the C═O group, respectively. The O 1s peak at 532.5 eV for the 5–15 s exposure is found to be broader (fwhm = 1.9 eV) than that at 531.8 eV (fwhm = 1.4 eV) for a thick film (5400 s). The larger width in the O 1s feature for a lower exposure is indicative of the existence of multiple components, including the carbonyl O at 532.1–532.9 eV and the hydroxyl O component at 532.8–534.4 eV.[32]

With increasing exposure to 45–2400 s, we observe the emergence and growth of a new N 1s feature at 401.1 eV (Figure 1b), attributable to N···H–O hydrogen bond (H-bond). Here we use "···" to denote a H-bond. This feature therefore indicates the formation of an interlayer vertical H-bond (head-to-tail) between a free carboxylic acid group of the interfacial layer (first adlayer) and a free amino group of the transitional layer (second adlayer), and that of intralayer horizontal (side-by-side) H-bond among two or more unidentate cysteine molecules (discussed below) in the interfacial layer. In Figure 2, we summarize the changes in the peak areas of the fitted XPS features. In particular, the N 1s intensity of the N···H–O feature for the 400 s exposure is ∼6 times that for 45 s exposure, which is consistent with the increase in the amount of vertical H-bonds for the 400 s exposure from that for the 45 s exposure, the latter with mostly horizontal H-bonds. The presence of both types of H-bonds is supported by the emergence of a second S 2s feature at 228.4 eV (Figure 1d) and of a fourth C 1s feature at 285.5 eV (Figure 1c) for the 45 s exposure, which are characteristic of the intact thiol (–SH) and thiol methyl ($-C_\beta H_2-SH$) groups, respectively. Moreover, there is a weak N 1s peak at ∼401.0 eV, which can be assigned to N···H–O feature.[10,11,33] For exposures in the transitional layer regime (i.e., above 45 s), the C 1s spectra have been fitted with four components at 284.5, 285.6, 286.6, and 289.2 eV, which are assigned to $-CH_2-S-Si$, $-CH_2-SH$, $-CH_2-NH-Si$, and –COOH, respectively.[17,20] Further exposure to 2400 s increases the N 1s intensity of the N···H–O feature for transitional layer ∼14 times with respect to that for the 45 s exposure (Figure 2a). Furthermore, close examination of Figure 2a represents that there is an increase in the N–H to S–H relative population from 50%:50% for 5 s exposure to 46%:54% for 45 s exposure. This is consistent with relative bond dissociation energies found for N–H (358.8 kJ/mol) and S–H bonds (353.6 kJ/mol).[34] Finally, the XPS spectra for the cysteine multilayers obtained for the 5400 s exposure on Si(111)7×7 are found to be similar to those for cysteine powders in the solid phase (Supporting Information, Figure S1). The shift of the peak maximum of the broad S 2s peak from 227.4 eV to that of the intact thiol peak at 228.4 eV

dx.doi.org/10.1021/ja509264t | J. Am. Chem. Soc. 2014, 136, 16909–16918

(Figure 1d) further affirms the multilayer nature. The sharp O 1s peak at 531.9 ± 0.1 eV (fwhm = 1.4 eV) (Figure 1a), and the single N 1s feature at 401.8 eV (Figure 1b) can only be assigned to, respectively, carboxylate ($-COO^-$) and protonated amino groups ($-NH_3^+$) in the zwitterionic structure ($NH_3^+CHCH_2SHCOO^-$, Scheme 1b) of the cysteine thick film (multilayers).[32] The corresponding C 1s spectrum (Figure 1c) consists of a broad band centered at 286.4 eV, attributable to the two alkyl carbons in $-CH_2-SH$ (at 285.9 eV) and $-CH-NH_3^+$ (at 286.8 eV), and a weaker feature at 288.8 eV corresponding to the carboxylate group.

To determine the thermal stability of the cysteine multilayer film (obtained with the 5400 s exposure) on the Si(111)7×7 surface, we anneal the sample for 600 s at elevated temperatures (85, 175, and 285 °C) and the sample is then cooled back to room temperature for XPS analysis. Annealing the sample at 85 °C evidently reduces the overall spectral intensities (Figure 2b), with the zwitterionic cysteine multilayer features significantly removed, which is indicated by the shifts of both the O 1s feature at 531.9 eV and the carboxyl C 1s feature at 288.8 eV to a higher binding energy and by the emergence of two N 1s features at 399.1 and 401.1 eV, corresponding to −NH−Si (of the interfacial layer) and the N···H−O H-bond, respectively (Figure 1). Furthermore, in the spectra evolution of the C 1s features of the cysteine film (Figure 1c), the position of the carboxyl C 1s feature is stable at 289.2 eV for the first and the second adlayers, but it shifts by 0.4 eV to a lower binding energy in the multilayers, while the position of C_β 1s feature (for the thiol-related carbon of the chemisorbed cysteine) is stable at 284.6 ± 0.1 eV for the interfacial and transitional layers. On the other hand, the position of C_α 1s feature is found to shift by 0.5 eV to a higher binding energy for the transitional layer upon H-bond formation. The resulting substantial reduction in the amount of physisorbed cysteine film is marked by the reappearance of the N 1s peak at 399.1 eV and the O 1s feature at 532.5 eV, corresponding to the aforementioned chemisorbed adspecies in the transitional and interfacial layers. Further annealing to 175 °C leads to complete desorption of the physisorbed multilayers and the reappearance of the chemisorption features, including the S 2s feature at 227.4 eV for S−Si bond and N 1s features at 401.1 eV for the N···H−O H-bond and at 400.0 eV for the free amino group. Annealing at high temperature also leads to decomposition of the adspecies to S atoms and other dissociated products. Finally, upon annealing at 285 °C, the S 2s peak shifts further to 226.8 eV and the C 1s, N 1s, and O 1s features closely resemble those found for the interfacial layer, that is, those obtained with 45 s exposure. By analogy to the thermal evolution of thiophene on Si(100)[35] and Pt(111),[36] we attribute the S 2s shift to the formation of atomic S on Si surface as a result of the C−S bond cleavage. By considering the stability of the thick cysteine nanofilm, we conclude that the zwitterionic structure can exist up to 85 °C, at which temperature conversion to transitional layer occurs. The transitional layer is more stable and could withstand annealing up to 175 °C. Between 175 and 285 °C, the −HN−Si bond remains intact. At or above 285 °C, the interfacial layer begins to break down, leading to dissociated S atoms on the Si surface. While the interfacial layer represents a very stable "permanent" adlayer, the transitional layer can be regarded as a renewable or "semi-permanent" one. The stabilities of these permanent and semipermanent adlayers provide the key to some interesting potential applications for drug delivery and medical applications.

We also obtain XPS spectra for the Si 2p feature of the substrate (Supporting Information, Figure S3). As expected, these spectra show that the intensity of the Si 2p feature decreases with increasing exposure time of cysteine because of the growing organic layer. Annealing causes partial removal of the cysteine film, which recovers the Si 2p intensity (as the organic layer becomes thinner). Furthermore, the absence of the silicon oxide feature at 103 eV confirms the cleanliness of the surface.

We further investigate the stability of the cysteine multilayer film (obtained with the 5400 s exposure) on Si(111)7×7 after storing at room temperature under ultrahigh vacuum conditions for 24, 72, and 120 h (Figure S4, Supporting Information, and Figure 2c). Evidently, after 24 h storage, there are 23%, 23%, and 29% reductions in the overall intensities for the respective N 1s, O 1s, and S 2s features, compared with the as-grown multilayer film (obtained with 5400 s exposure). These reductions indicate partial desorption of the thick zwitterionic film in ultrahigh vacuum over time. Interestingly, a weak N 1s feature is also observed at 399.1 eV, which corresponds to the emergence of the N−Si adstructures. By considering the intensity of protonated amino ($-NH_3^+$) peak, we conclude that the thickness of the zwitterionic cysteine film has been reduced to 44% after 120 h storage (Figure 2c). We repeat the same experiment for the transitional layer (obtained by annealing the multilayer film at 85 °C for 20 min) by storage under ultrahigh vacuum conditions for 48 and 120 h. As shown in Figure 2c (dashed lines), only a 10% reduction after 120 h storage is observed. This confirms that the transitional layer is considerably more stable than the zwitterionic multilayer. The transitional layer therefore offers a potentially robust platform for device fabrication and other applications requiring high vacuum conditions at room temperature.

The schematic in Figure 2d presents a summary of the bonding model of available surface functional groups and intra- and interlayer interactions for the interfacial layer, transitional layer, and the multilayer film of cysteine on Si(111)7×7 under ultrahigh vacuum conditions obtained by using the molecular beam epitaxy technique. Both the interfacial and transitional layers have been saturated by carboxylic acid and thiol groups, which could be used for binding with other adspecies. Since covalent Si−S and Si−N bonds in the interfacial layer are stronger than the vertical N···H−O H-bond between the interfacial and transitional layers, the interfacial layer should therefore require higher temperature to remove than the transitional layer. In contrast to interfacial and transitional layers, the surface of the zwitterionic multilayer is covered by thiol and protonated amino and deprotonated carboxylic acid groups, which leads to even weaker binding with other adspecies than the transitional layer.

To further investigate the nature and formation of these intra- and interlayer H-bonds in the interfacial and transitional layers, we conduct STM studies for the early growth stage. Figure 3 shows the corresponding filled-state and empty-state STM images (45 × 45 nm^2), collected, respectively, at −2 and +2 V sample bias with a 200 pA tunneling current, for a 3 s exposure of cysteine on Si(111)7×7. In these STM images, brightened features generally indicate saturation of the dangling bond sites with the addition of electron density from the adspecies. By comparing the filled-state image (Figure 3a, inset) with the corresponding empty-state image (Figure 3b, inset), we identify that each bright protrusion in a faulted half unit cell (up triangle) or an unfaulted half unit cell (down triangle)

dx.doi.org/10.1021/ja509264t | J. Am. Chem. Soc. 2014, 136, 16909−16918

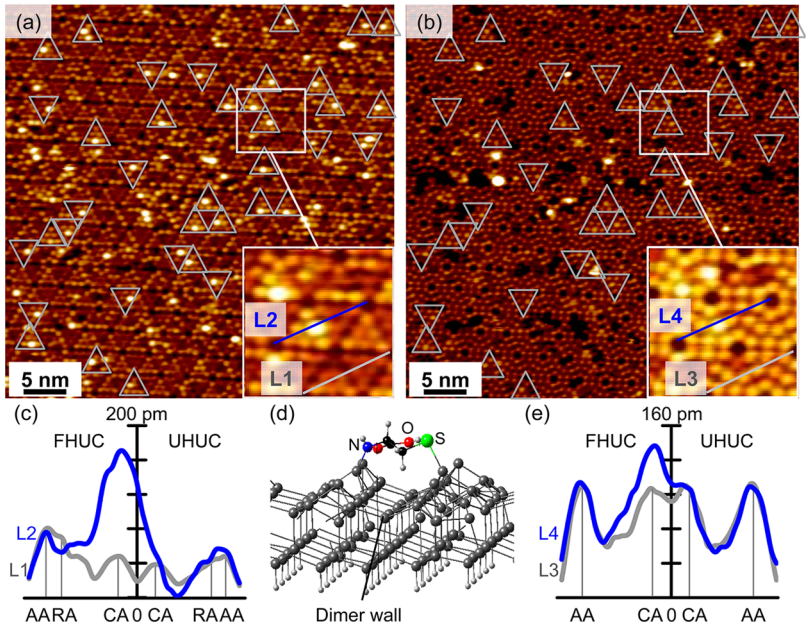

Figure 3. (a) Filled-state and (b) corresponding empty-state STM images (45 × 45 nm^2) for a 3 s exposure of cysteine on Si(111)7×7 obtained with a sample bias of −2 and +2 V, respectively, and a tunneling current of 200 pA, with magnified views (7.2 × 7.2 nm^2) shown in insets; and corresponding LDOS profiles along long diagonals [from corner atom (AA) to restatom (RA) and to center atom (CA)] (c) L1 and L2 and (e) L3 and L4, and (d) perspective view of the equilibrium geometry of a cysteine molecule adsorbed through N−H and S−H dissociation on adjacent center adatoms across a dimer wall on a $Si_{200}H_{49}$ slab as obtained by DFT calculation (Supporting Information). Cysteine molecules in the faulted (FHUC) and unfaulted half unit cells (UHUC) are marked with up triangles and down triangles, respectively. The separation between two adjacent center adatoms across a dimer wall is 0.677 nm.

represents a single cysteine adspecies on the Si(111)7×7 surface. The line profiles in Figure 3, panels c (L2) and e (L4), compare the local density of states (LDOS) differences at the marked positions of the corner adatom (AA), restatom (RA), and center adatom (CA) along the long diagonal in the reacted unit cell with those of the unreacted unit cell as indicated by the respective line profiles L1 and L3. Evidently, the bright protrusion in the magnified filled-state image (Figure 3a, inset) appears to cover two adatoms across the dimer wall, suggesting a bidentate adsorption arrangement involving a (CA, CA′) pair. We use parentheses to indicate a monomer in bidentate arrangement on two adatom sites, with a prime sign for the adatom in a different half unit cell. The corresponding LDOS profile of the bright protrusion along the long diagonal of the unit cell (Figure 3c, L2) further reveals the asymmetric LDOS located at a CA in the faulted half unit cell while clearly extending across the dimer wall to a CA in the unfaulted half unit cell, compared with that for an unreacted unit cell (L1). For the unreacted faulted half unit cell and unfaulted half unit cell (Figure 3a, inset), the LDOS at the CA site on the faulted half unit cell side is generally higher than that on the unfaulted half unit cell side and that the LDOS of the AA is higher than that of the CA within either half unit cell (Figure 3c, L1). On the other hand, the empty-state image (Figure 3b, inset) for the unreacted unit cell shows all adatoms with essentially the same LDOS (with similar brightness) on both the faulted half unit cell and unfaulted half unit cell (Figure 3e, L3). A higher LDOS is, again, evident at CA and the intensity is clearly extending into the dimer wall in L4 compared with L3 (Figure 3e). The protrusion for the occupied CA is however not dramatically brighter than other unoccupied atoms (e.g., AA). We will therefore concentrate our discussion on comparison between LDOS profiles along the long diagonals of the reacted (L2) and unreacted (L1) unit cells using the filled-state image in Figure 3c.

Evidently, the LDOS in the reacted unit cell is much higher (∼135 pm) than that in the unreacted one (Figure 3c). This asymmetric LDOS distribution suggests that cysteine is attached in either a bidentate configuration on the (CA, CA′) pair across the dimer wall through short-range interaction or a tilted unidentate configuration with a second longer-range interaction between a CA and one of the functional groups of the adsorbed cysteine molecule. This is consistent with the higher LDOS at the CA site in the reacted unfaulted half unit cell (L2) than that for the unreacted unfaulted half unit cell (L1), the "spillover" of which into the dimer wall also obscures the "valley" in the dimer wall. On the other hand, our complementary XPS results (Figure 1b,d) indicate a bidentate configuration through short-range interaction between the amino and thiol groups and Si adatoms at the lowest cysteine exposure (5−15 s). Furthermore, our large-scale DFT study of cysteine adsorption on a model Si(111)7×7 surface as represented by a $Si_{200}H_{49}$ slab concludes that the bidentate adstructure resulting from N−H and S−H dissociative adsorption of cysteine is considerably more stable than any unidentate adstructure. These results therefore provide strong support for our proposed bidentate adsorption structures for cysteine on Si(111)7×7 at the lowest exposure. Given that the separation between the NH_2 and OH groups in cysteine (3.66 Å) is too short to bridge two adatom sites across the dimer wall (6.77 Å), a larger separation between N and S (4.18 Å), obtained via N−H and S−H dissociation, would make such a bidentate configuration quite viable (Supporting Information, Figures S5−S7). Figure 3d shows a plausible equilibrium adstructure obtained by our DFT calculation, in which the free carboxylic acid group located on the faulted half unit cell side

dx.doi.org/10.1021/ja509264t | J. Am. Chem. Soc. 2014, 136, 16909−16918

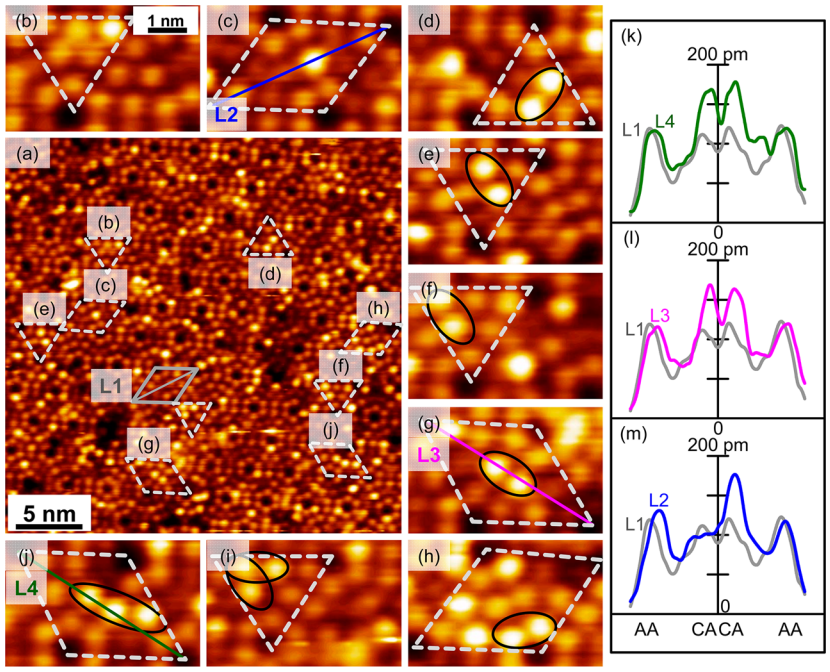

Figure 4. (a) Empty-state STM image (30 × 30 nm^2) of a 25 s exposure of cysteine on Si(111)7×7 recorded with a sample bias of +2 V and a tunneling current of 200 pA; magnified images of a bidentate cysteine molecule at (b) (AA, AA′) and (c) (CA, CA′) sites; H-bond mediated dimers formed from different unidentate cysteine molecules in (d) CA-CA in faulted half unit cell and (e) in unfaulted half unit cell, (f) AA-CA, (g) CA-CA′ (across the dimer wall), and (h) AA-AA′; self-assembled cysteine trimers in (i) CA-AA-CA and (j) CA-CA-CA′ sites on Si(111)7×7 surface. LDOS profiles along the long-diagonals (m) L2 for monomer in (c), (l) L3 for dimer in (g), and (k) L4 for trimer in (j), all compared with the LDOS profile L1 of the unreacted unit cell in panel a.

produces an asymmetric LDOS distribution across the dimer wall with a higher LDOS on the faulted half unit cell side. In the corresponding empty-state image (Figure 3b), we can also identify similar bright protrusions for the adsorbed cysteine molecule, but with a lower LDOS than that in the filled-state image. Furthermore, statistical analysis of these bright protrusions obtained for the lowest cysteine exposure (3 s) shows that the population of adstructures with the free carboxylic acid group on the faulted half unit cell side is 1.9 times that on the unfaulted half unit cell side, which suggests that formation of the stronger Si−N bond occurs more favorably on the more reactive faulted half unit cell.

The hydrogen atoms resulting from dissociative adsorption of cysteine are believed to adsorb on the restatom sites. This is in accord with previous studies of H_2 and NH_3 adsorption on Si(111)7×7 by Razado et al.[37] and by Zang et al.,[38] who reported that the dissociated hydrogen atoms adsorb on restatom sites. Because the topmost layer of the Si(111)7×7 surface (containing the adatoms) is more electrophilic in nature while the restatom layer is nucleophilic, the hydrogen atom would therefore adsorb on the nucleophilic restatom sites. The adsorption of hydrogen on restatom sites has also been observed for dissociative adsorption of other organic molecules, including glycine and glycylglycine, on Si(111)7×7.[14,15]

To follow the self-assembly process of adsorbed cysteine molecules, we show a 30 × 30 nm^2 empty-state image for a 25 s exposure of cysteine on Si(111)7×7 in Figure 4. While both empty-state and filled-state images of adsorbed cysteine on Si(111)7×7 appear similar (Figure 3a,b), the empty-state images are more straightforward to use for identifying the distribution of adspecies over the unit cells for higher cysteine exposures than the filled-state images. Evidently, a higher cysteine exposure increases the population of multiple adjacent bright protrusions, from dimers to trimers to multimers (Figure 4a), compared with very low exposure (Figure 3b). Closer examination reveals four types of dimers (D) and two types of trimer configurations (T) at this exposure: (D1) CA-CA and (D2) AA-CA, both within the same half unit cell (faulted half unit cell or unfaulted half unit cell); (D3) AA-AA′ and (D4) CA-CA′ across the dimer wall; (T1) CA-AA-CA (triangular trimer); (T2) CA-CA-CA′ (linear trimer). The formation of these clusters is clearly mediated by H-bonds. The CA-AA′ (across the dimer wall) dimer configuration is not observed, which is consistent with the large separation between CA and AA′ (10.25 Å) that is not conducive to H-bond formation.

Quite a few direct STM observations of the N···H−O H-bond in the self-assembly of amino acids have been reported in the literature.[14] The LDOS profiles along the long diagonals of the unit cells containing the (CA, CA′) monomer (Figure 4c, L2), CA-CA′ dimer (Figure 4g, L3), and CA-CA-CA′ trimer (Figure 4j, L4), in comparison to that for an unreacted a 7×7 unit cell (Figure 4a, L1), show the respective LDOS for one (L2), two (L3), and three (L4) cysteine molecules attached on adjacent CA adatoms. While the L2 profile of the (CA, CA′) monomer (Figure 4m, similar to L4 in Figure 3e) shows one bidentate cysteine molecule covering a (CA, CA′) pair across the dimer wall, the L3 profile of the CA-CA′ dimer (Figure 4l) clearly shows a valley in the LDOS at the dimer wall, with nearly the same LDOS at the CA sites in both faulted half unit cell and unfaulted half unit cell.

To complement our experimental findings, we also extended our large-scale DFT calculations to investigate different cysteine dimer adsorption configurations on Si(111)7×7 surface (Supporting Information). These dimer configurations are based in part on those of the gas-phase dimers, shown in the order of most stable to least stable in Schemes 1c−g. In

dx.doi.org/10.1021/ja509264t | J. Am. Chem. Soc. 2014, 136, 16909−16918

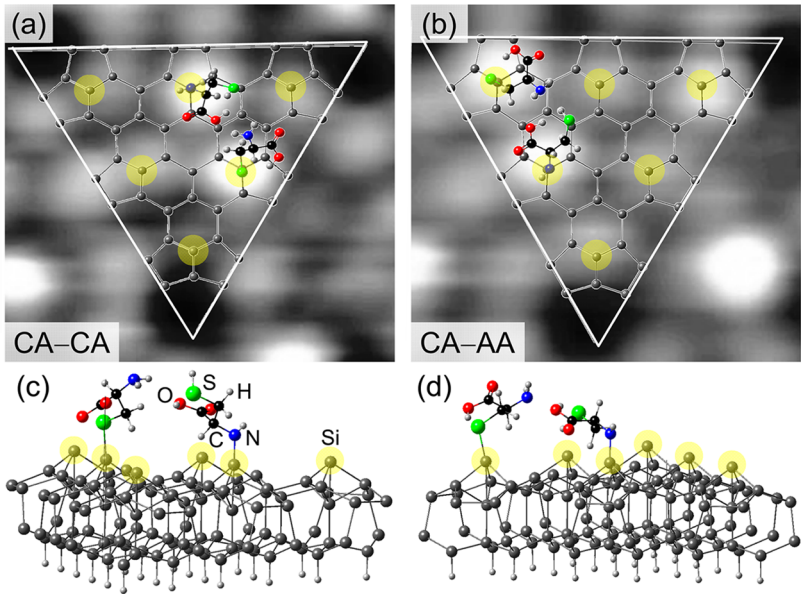

Figure 5. (a, b) Top views and (c, d) perspective views of equilibrium structures of cysteine dimer on (a, c) CA-CA and (b, d) CA-AA sites on a $Si_{200}H_{49}$ slab (used as a model Si(111)7×7 surface), as obtained from the DFT calculations, superimposed onto corresponding magnified empty-state STM images in panels a and b. Si adatoms are highlighted by larger yellow circles for clarity.

particular, there are five possible configurations for gas-phase cysteine dimers produced by formation of two O···H−O H-bonds (Scheme 1c), two S···H−N H-bonds (Scheme 1g), one O···H−O, and one N···H−O H-bonds (Scheme 1d), and of one of two single H-bonds, S···H−O (Scheme 1e) or N···H−N (Scheme 1f), between two adjacent cysteine molecules. The most stable dimer involves double O···H−O H-bonds between their carboxylic acid groups (Scheme 1c), while the least stable dimer contains just two S···H−N H-bonds between the amino and thiol groups (Scheme 1g; the bond energy for the O···H−O H-bond is 0.5 eV lower than that for S···H−N H-bond). The nominal (donor−acceptor) bond distances for a H-bond categorized as strong (mostly covalent), moderate (mostly electrostatic), and weak (electrostatic) bonds are 2.2−2.5 Å, 2.5−3.2 Å, and 3.2−4.0 Å, respectively.[39] As expected, the calculated H-bond distances in the most stable dimer formed by double O···H−O H-bonds between their carboxylic acid groups are discernibly shorter than that of strong H-bond due to the formation of cyclic dimer.

On the Si(111)7×7 surface, dimer formation is affected by steric hindrance on the adsorbed cysteine molecules exerted by the surface atoms, which rules out many of the gas-phase dimer configurations shown in Scheme 1. Our DFT calculations suggest that the N···H−O H-bond is a favorable H-bond that would lead to an acceptable cysteine dimer on adjacent CA-AA adatoms without torsion on the Si(111)7×7 surface. We overlay plausible configurations of such a cysteine dimer on the corresponding STM images of a CA-CA (Figure 5a) and CA-AA pair (Figure 5b). Perspective views of the corresponding equilibrium structures of these "torsion-free" dimer adsorption configurations are shown in Figure 5c,d. In these configurations, cysteine molecules are bound to the surface in unidentate fashion through S−H or N−H dissociative adsorption with the formation of the respective S−Si or N−Si bond. These unidentate adspecies allow the remaining unreacted functional groups freedom to interact with functional groups from a second cysteine adsorbed in an adjacent adatom site. This unidentate adsorption in effect leads to lateral interactions between a free amino group and a free carboxylic acid group, producing the N···H−O H bond. Our DFT study further shows that the donor−acceptor distances for these N···H−O H-bond configurations is 2.5−2.9 Å, in good accord with bond length of moderately strong H-bonds.

Figure 6a−d shows the empty-state images for four cysteine exposures on Si(111)7×7 in the build-up toward the transitional layer during the early growth stage (i.e., from 5 to 60 s exposure). Using the full 50 × 50 nm^2 images (of approximately 320 7×7 unit cells), we count the numbers of individual bidentate monomers, unidentate dimers, and trimers in order to estimate their relative surface concentrations (i.e., the fractions of available surface sites that are occupied by the respective cysteine configurations) and the total coverage, shown in Figure 6e. Evidently, growth begins with just the monomer and dimer populations on the 7×7 surface for the 5 s exposure (Figure 6a), with the relative surface concentration for monomers being discernibly higher than that for dimers, until they become nearly equal for the 20 s exposure. The surface concentration of the monomers increases sharply by 64% from 5 to 10 s exposure and then decreases slowly by 10% from 10 to 60 s exposure (Figure 6e, bottom panel). As the exposure increases, the relative surface concentrations for dimers and trimers increase gradually. The bar chart in Figure 6e (middle panel) shows the relative surface concentrations of various types of bidentate monomer configurations [corner adatom−corner adatom (AA, AA′) vs center adatom−center adatom (CA, CA′), both across the dimer wall], with increasing cysteine exposure. At the initial growth stage (5 s exposure), the relative surface concentration of the monomers with the (CA, CA′) configuration is found to be higher than that with the (AA, AA′) configuration, suggesting that the former configuration is more stable. This is consistent with the results from our large-scale DFT calculation, which also shows that the calculated adsorption energy of the adsorbed bidentate cysteine monomer on (CA, CA′) is 0.13 eV lower than that of the adsorbed cysteine on (AA, AA′) (Supporting Information, Figure S7). On the other hand, the population ratio of (CA,

dx.doi.org/10.1021/ja509264t | J. Am. Chem. Soc. 2014, 136, 16909−16918

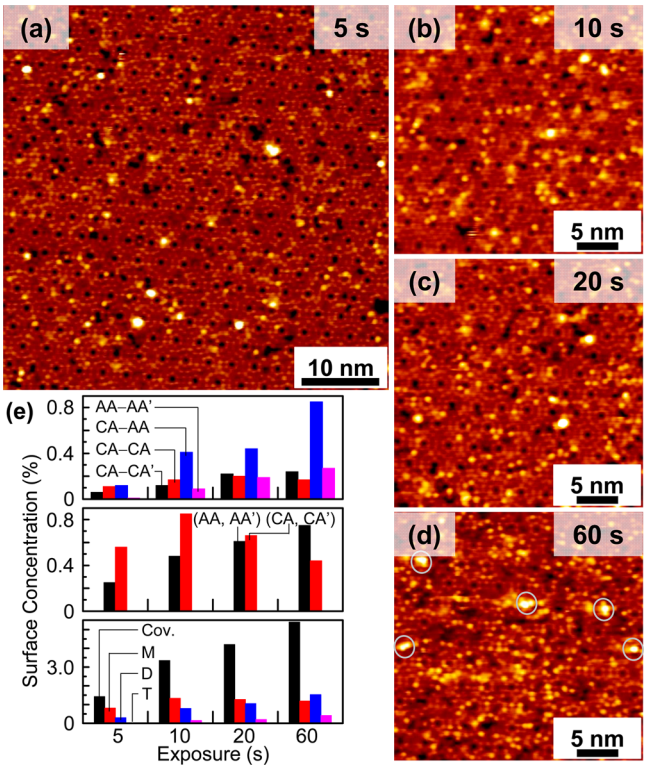

Figure 6. STM empty-state images collected at a sample bias +2 V and a tunneling current of 200 pA for cysteine exposures of (a) 5, (b) 10, (c) 20, and (d) 60 s on Si(111)7×7 surface and (e) (lower panel) the corresponding total coverage (Cov.) and the relative surface concentrations for monomer (M), dimer (D) and trimer (T) configurations, (middle and upper panels) various type of respective M and D configurations on Si(111)7×7 sites.

CA′) to (AA, AA′) is decreasing gradually as a result of formation of dimer and trimer configurations. For the lowest exposure (5 s) of cysteine, the relative surface concentrations of the more popular types of dimer configurations follow the ordering: CA-AA > CA-CA > CA-CA′ > AA-AA′ (Figure 6e, top panel). There are steady increases in the CA-AA and AA-AA′ surface concentrations, while the CA-CA and CA-CA′ surface concentrations appear to be leveling off with increasing exposure to above 10 s, which could be the result of increasing population of the trimer (CA-CA-CA′) configuration. This evolution of the dimer growth is consistent with the more reactive CA sites being occupied first. Based on our STM and XPS results, the coverage-dependent adsorption configurations of cysteine molecules on the Si(111)7×7 surface play an important role in the observed evolution of the surface concentrations of these multimers. At very low cysteine exposure, preferential bidentate monomer adsorption on the (CA, CA′) sites (across the dimer wall) is observed, while formation of H-bond between the unidentate cysteine molecules becomes predominant at higher exposure. Moreover, at higher exposure (60 s, marked by circles in Figure 6d), we can see the emergence of brighter, larger protrusions, which suggest the on-set of the translational layer growth, with larger clusters arising from formation of vertical H-bonds between a free carboxylic acid group from the first adlayer and an amino group of the second adlayer. Furthermore, the growth of the translational layer begins before formation of the complete interfacial layer.

CONCLUSION

The growth evolution of cysteine on Si(111)7×7 at room temperature in ultrahigh vacuum conditions has been studied by combining XPS chemical-state data with STM LDOS images. Three N 1s features for N−Si at 398.7 eV, N···H−O at 401.1 eV, and $-NH_3^+$ at 401.8 eV are found to emerge sequentially with increasing deposition time, which mark the onsets of three distinct growth stages. In the formation of the interfacial layer (first stage), cysteine is found to undergo N−H and S−H dissociative adsorption and form a bidentate adstructure across the dimer wall of the 7×7 surface. Both filled-state and empty-state STM images reveal the presence of bright protrusions over the (CA, CA′) adatom sites across the dimer wall, which correspond to asymmetric LDOS resulting from the off-to-side orientation of the free carboxylic acid group. As the exposure increases, more unidentate cysteine adstructures bonded through Si−N or Si−S are found. The corresponding bright protrusions begin to self-assemble into dimer, trimer, and higher-order multimer configurations. The formation of these self-assembled arrangements is driven by horizontal H-bonding between a free carboxylic acid group and an amino group of adjacent cysteine molecules. These unidentate adstructures leave the carboxylic acid group free to engage other incoming moieties, and the interfacial layer is found to be very stable and breaks down only at 285 °C (the maximum annealing temperature employed in the present work). For a higher exposure, we observe the formation of vertical N···H−O H-bonds, signaling the onset of a transitional layer (second stage),[10,11,33] which is found to be stable to 175 °C. The final stage is marked by formation of a cysteine multilayer film in zwitterionic form ($NH_3^+CHCH_2SHCOO^-$). This study shows that a highly reactive Si surface, full of Si dangling bonds, can be easily converted to different types of bio-organic surfaces. These surfaces, with both carboxylic acid and thiol groups free to serve as receptor sites for incoming moieties, offer potential applications in biosensing and heavy metal detection. Because the transitional layer is held to the interfacial layer by weak H-bonding, this layer offers a "renewable" platform for sensing application.

ASSOCIATED CONTENT

Supporting Information

Additional XPS results for cysteine multilayer films and powder, binding energies of spectral features at different exposure and annealing temperature, S 2p and Si 2p XPS spectra, and details and results of large-scale DFT calculations. This material is available free of charge via the Internet at http://pubs.acs.org.

AUTHOR INFORMATION

Corresponding Author

tong@uwaterloo.ca

Notes

The authors declare no competing financial interest.

ACKNOWLEDGMENTS

This work was supported by the Natural Sciences and Engineering Research Council of Canada.

REFERENCES

(1) Hamers, R. J.; Coulter, S. K.; Ellison, M. D.; Hovis, J. S.; Padowitz, D. F.; Schwartz, M. P.; Greenlief, C. M.; Russell, J. N. *Acc. Chem. Res.* **2000**, 33 (9), 617−624.

(2) Leftwich, T. R.; Teplyakov, A. V. *Surf. Sci. Rep.* **2008**, *63*, 1−71.
(3) Filler, M. A.; Bent, S. F. *Prog. Surf. Sci.* **2003**, *73* (1−3), 1−56.
(4) Mayne, A. J.; Riedel, D.; Comtet, G.; Dujardin, G. *Prog. Surf. Sci.* **2006**, *81* (1), 1−51.
(5) Buriak, J. M. *Chem. Rev.* **2002**, *102* (5), 1271−1308.
(6) Wang, X.; Landis, E. C.; Franking, R.; Hamers, R. J. *Acc. Chem. Res.* **2010**, *43* (9), 1205−1215.
(7) Tao, F.; Bernasek, S. L.; Xu, G.-Q. *Chem. Rev.* **2009**, *109* (9), 3991−4024.
(8) Tao, F.; Xu, G. Q. *Acc. Chem. Res.* **2004**, *37* (11), 882−893.
(9) Rahsepar, F. R.; Zhang, L.; Leung, K. T. *J. Phys. Chem. C* **2014**, *118* (17), 9051−9055.
(10) Zhang, L.; Chatterjee, A.; Ebrahimi, M.; Leung, K. T. *J. Chem. Phys.* **2009**, *130* (12), No. 121103.
(11) Zhang, L.; Chatterjee, A.; Leung, K. T. *J. Phys. Chem. C* **2011**, *115* (29), 14155−14163.
(12) Chatterjee, A.; Zhang, L.; Leung, K. T. *Langmuir* **2013**, *29* (30), 9369−9377.
(13) Chatterjee, A.; Zhang, L.; Leung, K. T. *J. Phys. Chem. C* **2013**, *117* (28), 14677−14683.
(14) Chatterjee, A.; Zhang, L.; Leung, K. T. *J. Phys. Chem. C* **2012**, *116* (20), 10968−10975.
(15) Chatterjee, A.; Zhang, L.; Leung, K. T. *Langmuir* **2012**, *28* (34), 12502−12508.
(16) Uvdal, K.; Bodo, P.; Liedberg, B. *J. Colloid Interface Sci.* **1992**, *149* (1), 162−173.
(17) Fischer, S.; Papageorgiou, A. C.; Marschall, M.; Reichert, J.; Diller, K.; Klappenberger, F.; Allegretti, F.; Nefedov, A.; Wöll, C.; Barth, J. V. *J. Phys. Chem. C* **2012**, *116* (38), 20356−20362.
(18) Kühnle, A.; Linderoth, T. R.; Hammer, B.; Besenbacher, F. *Nature* **2002**, *415* (6874), 891−893.
(19) Ataman, E.; Isvoranu, C.; Knudsen, J.; Schulte, K.; Andersen, J. N.; Schnadt, J. *Surf. Sci.* **2011**, *605* (1−2), 179−186.
(20) Huang, J. Y.; Ning, Y. S.; Yong, K. S.; Cai, Y. H.; Tang, H. H.; Shao, Y. X.; Alshahateet, S. F.; Sun, Y. M.; Xu, G. Q. *Langmuir* **2007**, *23* (11), 6218−6226.
(21) Gross, D.; Grodsky, G. *J. Am. Chem. Soc.* **1955**, *77* (6), 1678−1680.
(22) NIST Chemistry WebBook. http://webbook.nist.gov/chemistry.
(23) Fernández-Ramos, A.; Cabaleiro-Lago, E.; Hermida-Ramón, J. M.; Martínez-Núñez, E.; Peña-Gallego, A. *J. Mol. Struct. THEOCHEM* **2000**, *498* (1−3), 191−200.
(24) Dobrowolski, J. C.; Rode, J. E.; Sadlej, J. *J. Mol. Struct. THEOCHEM* **2007**, *810* (1−3), 129−134.
(25) He, J.; Patitsas, S. N.; Preston, K. F.; Wolkow, R. A.; Wayner, D. D. M. *Chem. Phys. Lett.* **1998**, *286* (5), 508−514.
(26) Cao, X.; Hamers, R. J. *J. Am. Chem. Soc.* **2001**, *123* (44), 10988−10996.
(27) Huang, H. G.; Huang, J. Y.; Ning, Y. S.; Xu, G. Q. *J. Chem. Phys.* **2004**, *121* (10), 4820−4825.
(28) Cao, X.; Coulter, S. K.; Ellison, M. D.; Liu, H.; Liu, J.; Hamers, R. J. *J. Phys. Chem. B* **2001**, *105* (18), 3759−3768.
(29) Kugler, Th.; Thibaut, U.; Abraham, M.; Folkers, G.; Gopel, W. *Surf. Sci.* **1992**, *260*, 64−67.
(30) Pauling, L. *The Nature of the Chemical Bond and the Structure of Molecules and Crystals*, 3rd ed.; Cornell University Press: Ithaca, NY, 1960, Vol. *148*.
(31) Coulter, S. K.; Schwartz, M. P.; Hamers, R. J. *J. Phys. Chem. B* **2001**, *105* (15), 3079−3087.
(32) Clark, D. T.; Peeling, J.; Colling, L. *Biochim. Biophys. Acta* **1976**, *453*, 533−545.
(33) Zhang, L.; Chatterjee, A.; Leung, K. T. *J. Phys. Chem. Lett.* **2010**, *1* (23), 3385−3390.
(34) Kerr, J. A. In *CRC Handbook of Chemistry and Physics*, 81st ed.; Lide, D. R., Ed.; CRC Press: Boca Raton, FL, 2000.
(35) Qiao, M. H.; Cao, Y.; Tao, F.; Liu, Q.; Deng, J. F.; Xu, G. Q. *J. Phys. Chem. B* **2000**, *104* (47), 11211−11219.
(36) Stöhr, J.; Gland, J. L.; Kollin, E. B.; Koestner, R. J.; Johnson, A. L.; Muetterties, L.; Sette, F. *Phys. Rev. Lett.* **1984**, *53* (22), 2161−2164.
(37) Razado, I. C.; Zhang, H. M.; Uhrberg, R. I. G.; Hansson, G. V. *Phys. Rev. B* **2005**, *71* (23), No. 235411.
(38) Zang, K.; Guo, Q.; Fu, H.; Yu, Y.; Qin, Z.; Cao, G. *J. Phys.: Condens. Matter* **2010**, *22* (8), No. 085002.
(39) Jeffrey, G. A. *An Introduction to Hydrogen Bonding*; Oxford University Press: New York, 1997; Vol. *6*, p 320.